AL/HR-TP-1997-0029

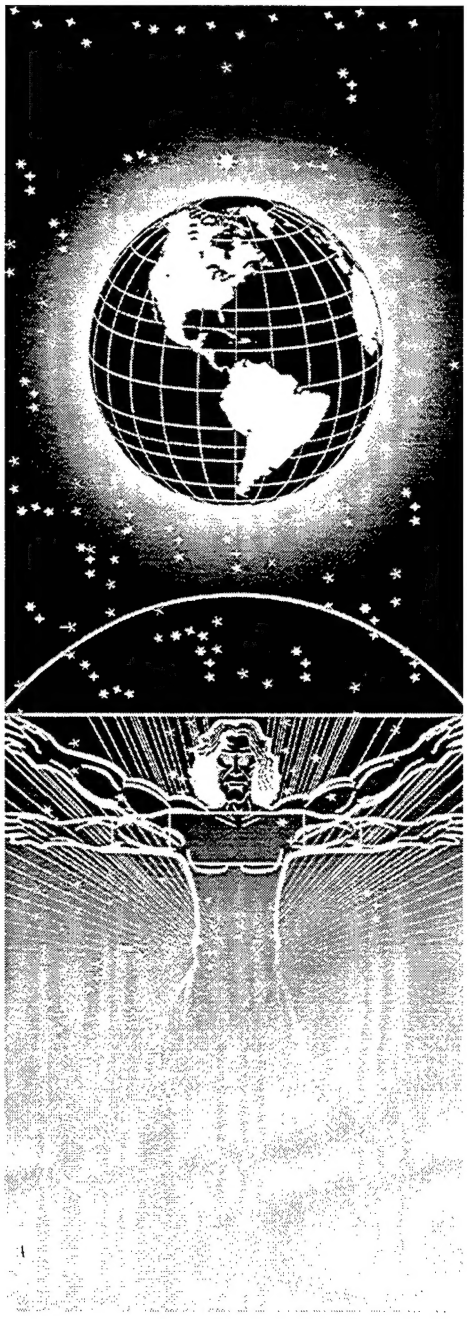

UNITED STATES AIR FORCE ARMSTRONG LABORATORY

Neural Network Technology for the Rapid Identification of Corrosion Damage in Aging Aircraft

Paul M. Hartke
Steven C. Gustafson
Theresa A. Tuthill

University of Dayton Research Institute
300 College Park Drive
Dayton, Ohio 45469

Shing P. Chu

HUMAN RESOURCES DIRECTORATE
LOGISTICS RESEARCH DIVISION
2698 G Street
Wright-Patterson AFB OH 45433-7604

May 1997

Human Resources Directorate
Logistics Research Division
2698 G Street
Wright-Patterson AFB OH 45433-7604

NOTICES

When Government drawings, specifications, or other data are used for any purpose other than in connection with a definitely Government-related procurement, the United States Government incurs no responsibility or any obligation whatsoever. The fact that the Government may have formulated or in any way supplied the said drawings, specifications, or other data, is not to be regarded by implication, or otherwise in any manner construed, as licensing the holder, or any other person or corporation, or as conveying any rights or permission to manufacture, use, or sell any patented invention that may in any way be related thereto.

The Public Affairs Office has reviewed this report, and it is releasable to the National Technical Information Service, where it will be available to the general public, including foreign nationals.

This paper has been reviewed and is approved for publication.

SHING P. CHU
Project Scientist

BERTRAM W. CREAM, Chief
Logistics Research Division

REPORT DOCUMENTATION PAGE

Form Approved
OMB No. 0704-0188

1. AGENCY USE ONLY (Leave blank)	2. REPORT DATE	3. REPORT TYPE AND DATES COVERED
	May 1997	Final Technical Paper - Mar 1996 to Aug 1996

4. TITLE AND SUBTITLE

NEURAL NETWORK TECHNOLOGY FOR THE RAPID IDENTIFICATION OF CORROSION DAMAGE IN AGING AIRCRAFT

5. FUNDING NUMBERS

C - SPO900-94-D-0001, DO 5
PE - 62205F
PR - 1710
TA - D0
WU - 03

6. AUTHOR(S)

Paul M. Hartke
Theresa A. Tuthill
Steven C. Gustafson
Shing P. Chu

7. PERFORMING ORGANIZATION NAME(S) AND ADDRESS(ES)

University of Dayton Research Institute
CSERIAC Program Office
AL/CFH/CSERIAC, Bldg. 248
2255 H Street
Wright-Patterson AFB OH 45433-7022

8. PERFORMING ORGANIZATION REPORT NUMBER

AL/HR-TP-1997-0029

9. SPONSORING/MONITORING AGENCY NAME(S) AND ADDRESS(ES)

Armstrong Laboratory
Logistics Research Division
2698 G Street
Wright-Patterson AFB OH 45433-7604

10. SPONSORING/MONITORING AGENCY REPORT NUMBER

11. SUPPLEMENTARY NOTES

Armstrong Laboratory Project Scientist: Shing P. Chu, AL/HRGO, (513) 255-3871

12a. DISTRIBUTION/AVAILABILITY STATEMENT

Approved for public release; distribution is unlimited

12b. DISTRIBUTION CODE

13. ABSTRACT ***(Maximum 200 words)***

Corrosion damage in aging aircraft is an increasingly critical concern for the U. S. Air Force. Effective, but inexpensive, techniques are needed to identify and evaluate corrosion damage to aircraft structures . The extent of material loss due to corrosion can be reliably measured from x-ray data, but x-ray measurements are costly, slow, and usually require significant aircraft disassembly. Corrosion by-products, which typically occupy more volume than uncorroded material, often causes slight aircraft surface deformations, or "pillowing." Pillowing can be measured with various inexpensive, rapid, and nondestructive optical imaging techniques. However, the relationship between percent material loss and "pillowing" surface deformation is complex, and conventional methods for quantifying the relationship typically lead to unacceptably low correct-detection rates or unacceptably high false-alarm rates. Neural net technology offers a potentially more accurate approach for establishing this relationship. This paper describes the results of a study applying neural net technology to evaluate the percent of material loss and pillowing surface deformation measured with optical imaging techniques.

14. SUBJECT TERMS

artificial neural network
nondestructive inspection/evaluation
pattern recognition
radial basis function
NDI/E
corrosion pillowing

15. NUMBER OF PAGES

17

16. PRICE CODE

17. SECURITY CLASSIFICATION OF REPORT	18. SECURITY CLASSIFICATION OF THIS PAGE	19. SECURITY CLASSIFICATION OF ABSTRACT	20. LIMITATION OF ABSTRACT
Unclassified	Unclassified	Unclassified	SAR

CONTENTS

FIGURES

ACKNOWLEDGMENTS

This work was initiated through and supported in part by a contract with the U. S. Air Force Armstrong Laboratory AL/HRGO; P. Chu, N. Cox, and B. Elnamara were the technical monitors. Additional support was provided by the U.S. Air Force Wright Laboratory WL/MLIM; S. LeClair was the technical monitor. C. Buynak of WL/MLLP identified the problem addressed in this work and located the required data, which was provided through M. Howard of ARINC. Helpful discussions with and suggestions from all of the above are gratefully acknowledged, as are inputs from J. Brausch of WL/MLSA, J. Whitaker of OCALC, R. Andrews and L. Quill of the University of Dayton, O. Hageniers and F. Karpala of Diffracto Ltd., J. Komorowski of NRC Canada, and K. Harding of The Industrial Technology Institute, Ann Arbor, Michigan.

INTRODUCTION

This paper will present the progress of an effort sponsored by the Armstrong Laboratory's Human Resources Logistics Research Division - Operations Branch (HRGO) which examined the process of identifying corrosion data in aircraft using neural network optical image processing techniques. Corrosion damage in aircraft is becoming a critical concern for the US Air Force due to the increasing age of typical operational aircraft; i.e., among other factors, fewer types and numbers of new aircraft are being produced. For example, an issue with the aging C/KC-135 aircraft fleet is the hidden corrosion in lap joints. X-ray techniques that determine percent material loss due to corrosion are perhaps the most reliable methods for assessing corrosion damage, but they are costly, slow, and usually require significant aircraft disassembly.

For corrosion near aircraft exterior surfaces, corrosion by-products, which generally occupy more volume than uncorroded material, often cause slight surface deformations or "pillowing" that can be measured with various relatively inexpensive, rapid, and nondestructive optical imaging techniques (Karpala and Hageniers, 1995). However, the relationship between percent material loss and "pillowing" surface deformation is complex, and conventional methods for quantifying the relationship generally lead to unacceptably low correct-detection probabilities or unacceptably high false-call probabilities for the identification of corrosion from optical data (Howard, Mitchell, and Tietz, 1995).

This paper considers the significantly more reliable relationship that might be established using neural network technology.

BACKGROUND

D-Sight is a large-area corrosion detection technique from the Diffracto Ltd., in Windsor, Ontario, Canada. This technique is recognized for its ability to detect pillowing. However, as a rapid visualization technique dependent on the operator's experience and judgment, it suffers from a high false call rate. Neural network techniques may lead to better interpretation of the data and thus result in reduced false call rates. This in turn will lead to significant benefits for the Air Force by eliminating unnecessary maintenance activities.

METHODS

The results that characterize this possible advance are based on both x-ray and optical data from an actual aircraft lap joint test coupon (coupon F) that has significant corrosion damage. The x-ray data has gray scale proportional to percent material loss, and this gray scale is the "truth" against which the optical data is compared. The optical data is from a commercial "enhanced visual" system in which vertical surface deformations (which may be due in part to corrosion-induced "pillowing") are rendered as image gray scale variations.

RESULTS

This section will present the results through a series of figures from an actual corroded aircraft lap joint. Figures 1 to 4 present the reference data upon which various spatial frequency filters are tested for their ability to distinguish corrosion effects. Both static (figures 5 to 10) and adaptive filter (figures 11 to 13) processing techniques were assessed.

X-ray and Optical Data

Figure 1 shows the x-ray data for the lap joint test coupon. The black regions indicate fastener locations. The remaining gray scale is proportional to percent material loss due to corrosion. The percent material loss is generally greater than 15 percent except in the boxed region. This boxed area has much less percentage loss over approximately the right-most 60 percent of its area.

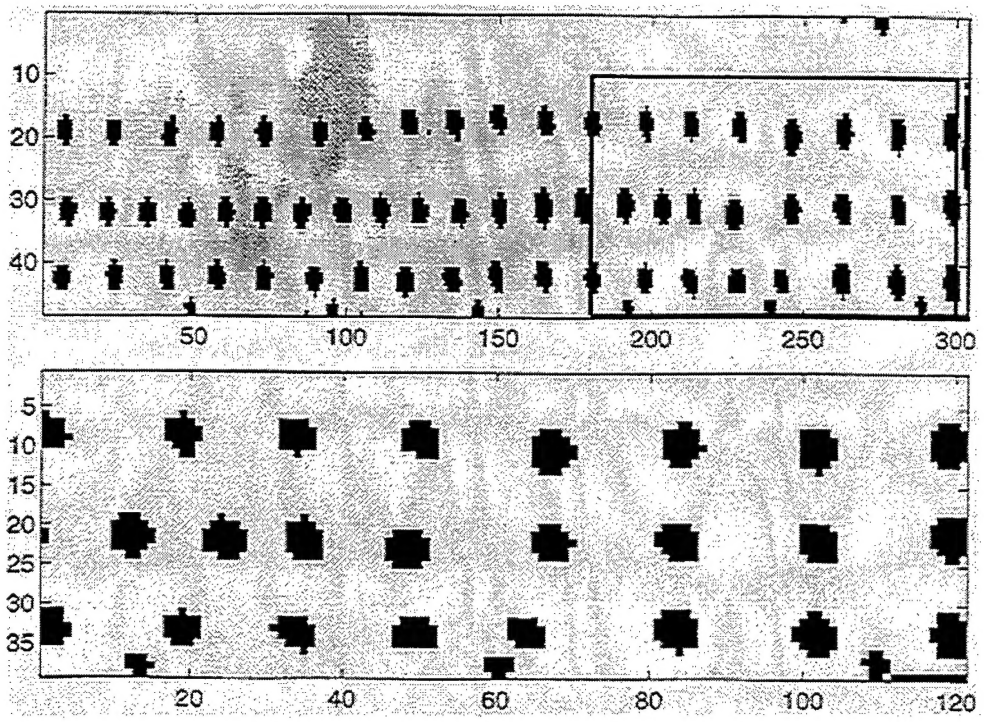

Figure 1. X-ray Data: Overview (top), Boxed Region (bottom)

Figure 2 shows the optical data for the lap joint test coupon. In this figure, gray scale has a component related to vertical surface deformation, but the proportionality is nonlinear as is evident from the crater-like appearance of the fastener locations. The same boxed region indicated in Figure 1 is shown here (right). Note however, that the aspect angle, size (in both length and width), and resolution (i.e., number of pixels) differs for the x-ray and optical data.

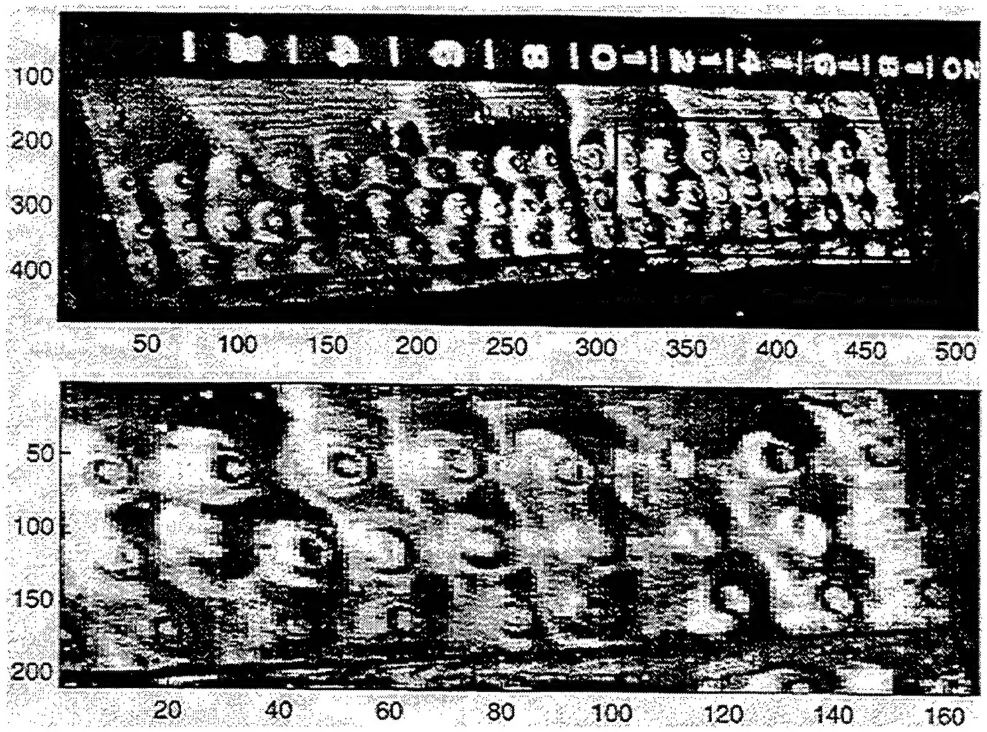

Figure 2. Optical Data: Overview (top), Boxed Region (bottom).

Figure 3 shows the x-ray data in the boxed region linearly transformed to cover a 100 by 200 pixel region and plotted in both gray scale and surface profile formats. Figure 4 shows the optical data in the same boxed region also linearly transformed (including rotation to a normal aspect angle) to cover the same 100 by 200 pixel region and also plotted in both gray scale and surface profile formats.

These two figures contain the data to be related using neural network (or perhaps other more effective) technology. Note that there is no apparent qualitative ("by eye") relationship. Visual inspection clearly indicates that on the left portion of the x-ray there is corrosion; whereas the right portion shows little or no corrosion (Figure 3). However, the optical data do not visually indicate the same pattern of results.

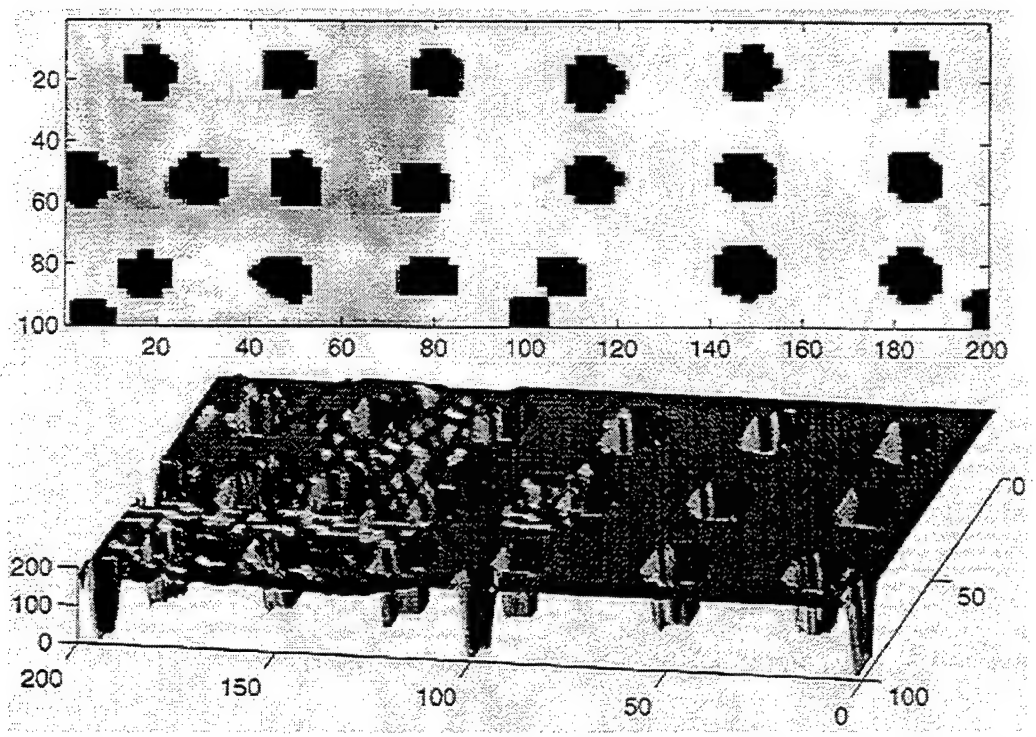

Figure 3. Transformed X-ray Data: Gray Scale Plot (top), Surface Profile Plot (bottom).

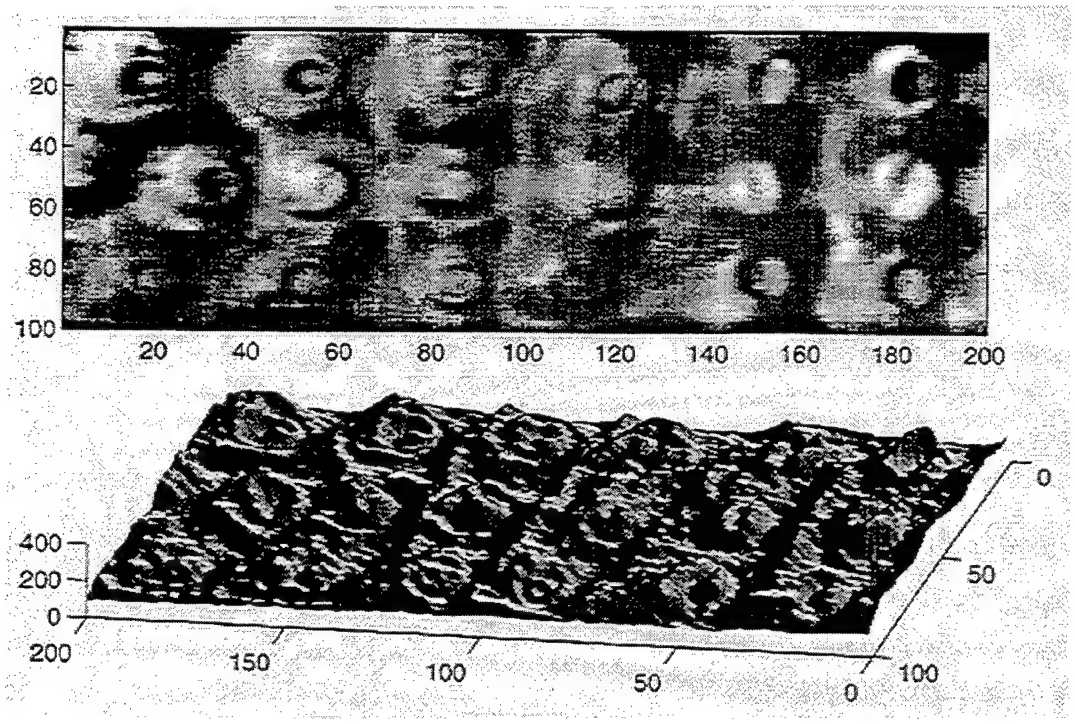

Figure 4. Transformed Optical Data: Gray Scale Plot (top), Surface Profile Plot (bottom).

Static Filter Processing

It is clear from Figures 3 and 4 that a successful supervised-learning neural network (or other processor) would distinguish the right-most 60 percent of the optical data area as relatively uncorroded compared to the remaining area. Accordingly, several low pass, high pass, and band pass spatial frequency filters (which may be regarded as a priori-trained neural networks) are tested for their ability to make this distinction.

Figure 5 shows the optical data of Figure 4 displayed in four contour plots with different numbers of contour lines from minimum to maximum gray level. High contour line densities indicate regions with relatively high spatial frequencies (i.e., steep slopes), and the identification of these regions could be valuable in the selection of appropriate filters. However, none of the contour plots display a significant and consistent contour line density increase or decrease in the right most 60 percent of the data area.

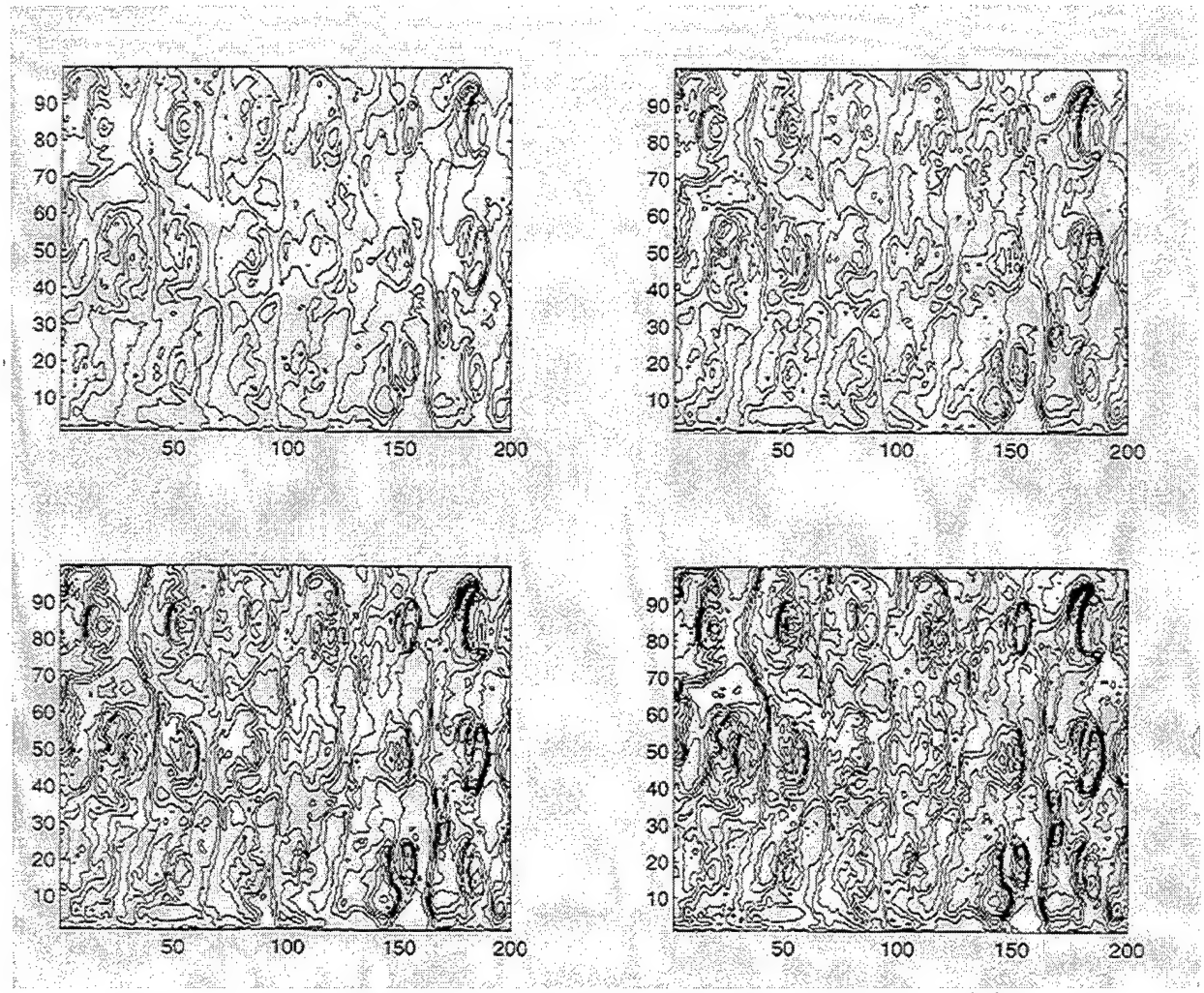

Figure 5. Contour Plots for Transformed Optical Data: 6 Contours Minimum to Maximum (top, L), 8 Contours (top, R), 10 Contours (bottom, L), 12 Contours (bottom, R).

Figure 6 shows the impulse response whose Fourier transform best approximates a low pass filter that retains all spatial frequencies below 25 percent of the full frequency range when this impulse response is constrained to have zero values beyond an 11 by 11 pixel region. Figure 7 shows a contour plot for the transformed optical data processed with this filter and with a similar low pass filter with an approximate cutoff of 75 percent. Figures 8 and 9 show similar plots for high pass and band pass filters, respectively; in each case the impulse response was constrained to have zero values beyond an 11 by 11 pixel region and the stated percentages indicate the cutoff value or bandpass region.

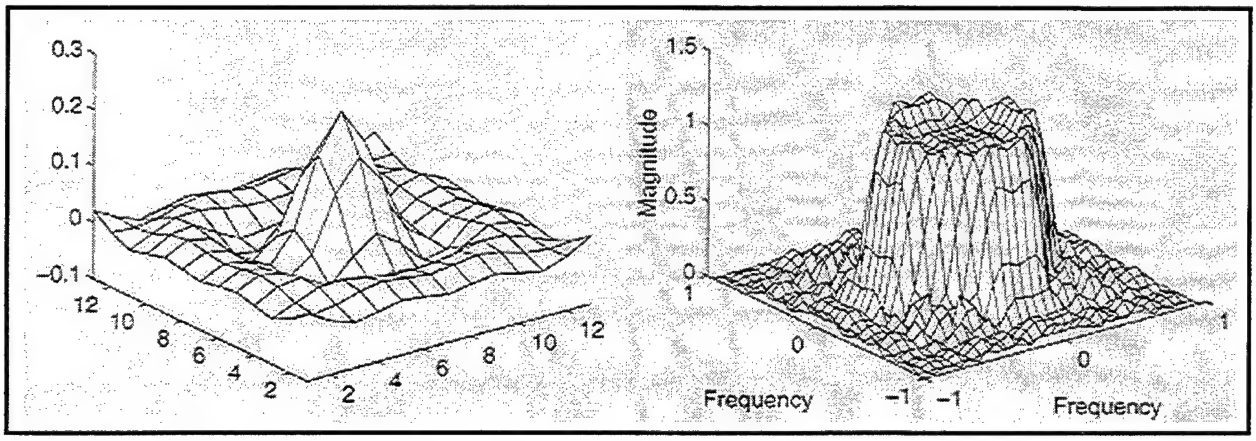

Figure 6. Impulse Response Limited to 11 by 11 Pixels (left), Corresponding Best-Approximation 25 Percent Low Pass Filter (right).

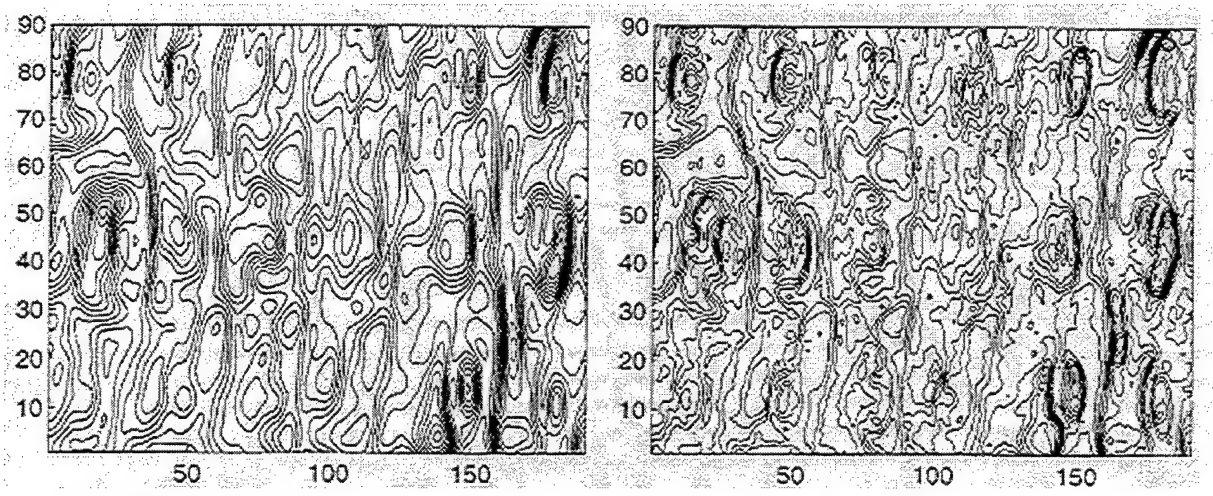

Figure 7. Contour Plots (12 Contours) for Transformed Optical Data Processed with Low Pass Filters: 25 Percent Approximate Cutoff (left), 50 Percent Approximate Cutoff (right).

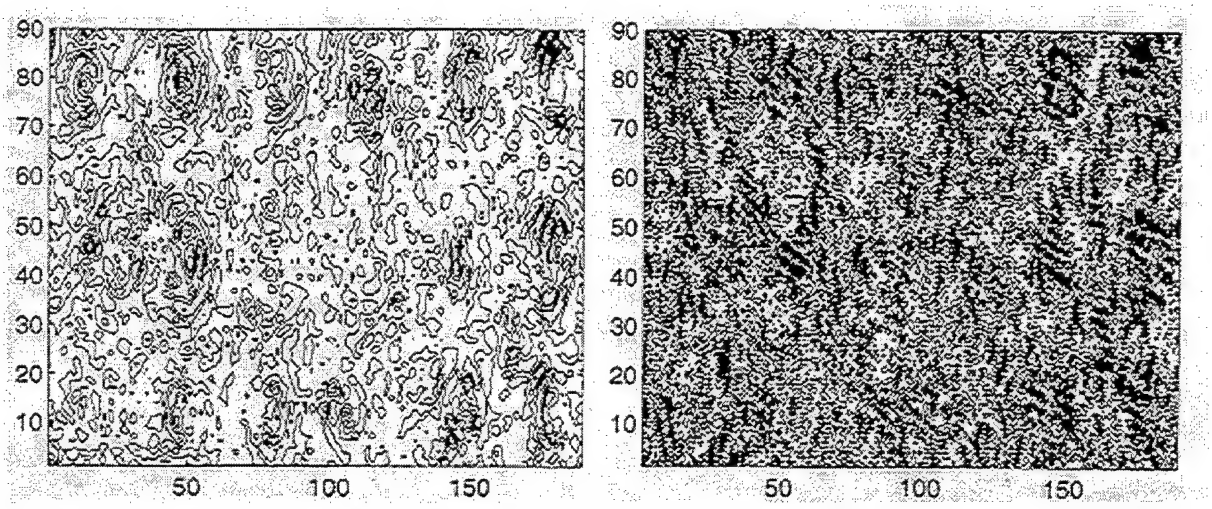

Figure 8. Contour Plots (12 Contours) for Transformed Optical Data Processed with High Pass Filters: 25 Percent Approximate Cutoff (left), 75 Percent Approximate Cutoff (right).

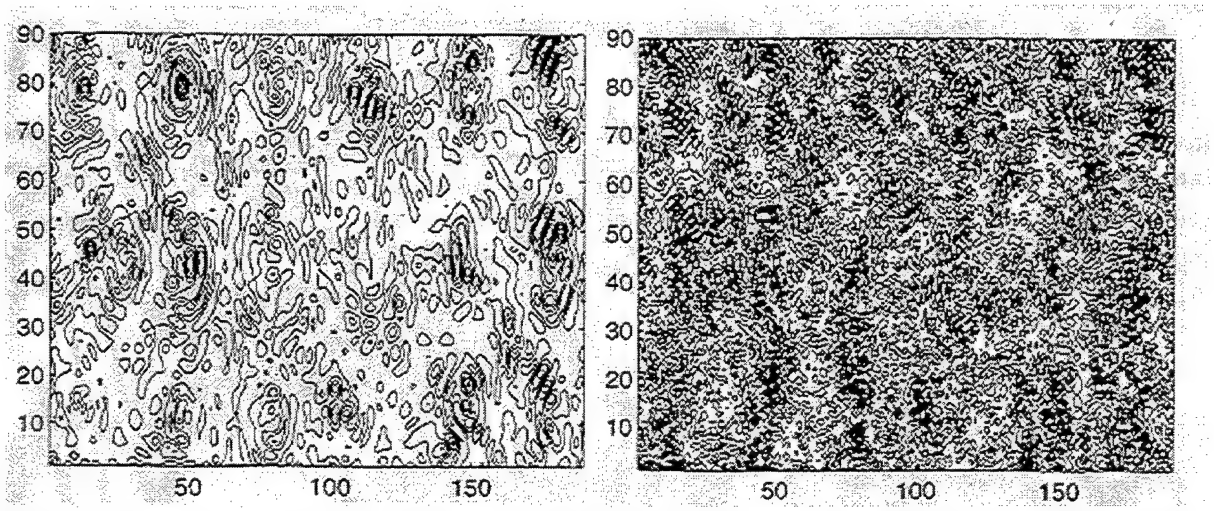

Figure 9. Contour Plots (12 Contours) for Transformed Optical Data Processed with Bandpass Filters: 25 Percent to 50 Percent Approximate Range (left), 50 Percent to 75 Percent Approximate Range (right).

Finally, Figure 10 shows contour plots for the transformed optical data after processing with one of two smooth-cutoff filters. One plot corresponds to a uniform impulse response and the other corresponds to a Gaussian impulse response of 1.5 pixel standard derivation, where both impulse responses are constrained to have zero values beyond a 5 by 5 pixel region. Again, none of the contour plots tends to display the desired significant and consistent contour line density increase or decrease in the right-most 60 percent of the data area.

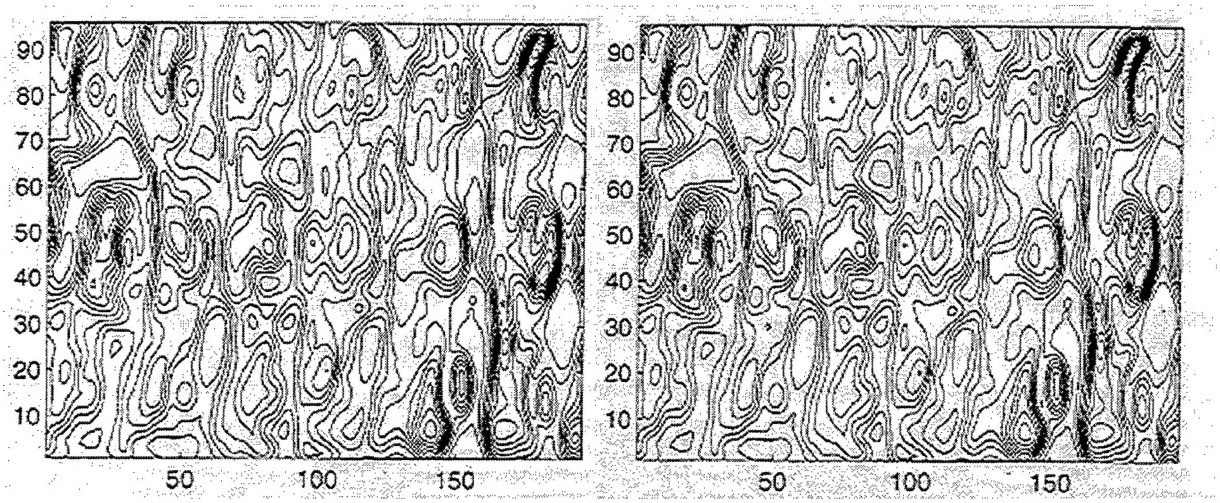

Figure 10. Contour Plots (12 Contours) for Transformed Optical Data Processed with Smooth-Cutoff Filters: Uniform Impulse Response over 5 by 5 Pixels (left), Gaussian Impulse Response with 1.5 Pixel Standard Deviation (right).

Adaptive Filter Processing

Since static filter processing proved to be ineffective (at least for the tested filters) in relating the x-ray (training) and optical (testing) data, adaptive filter processing with the filter synthesized using a radial basis function neural network technology (Ripley, 1996) was attempted. The objective was to find a "custom" filter that, when applied to the transformed optical data, would demonstrate a significant and consistent contour line density increase or decrease in the right-most 60 percent of the data area. The synthesis (or training) procedure was as follows:

(a) Locate eight 16 by 16 pixel arrays on the 100 by 200 pixel transformed optical data so that fastener pixels are avoided and so that four of the arrays are in the rightmost 60 percent of the data area (i.e., the relatively uncorroded area).

(b) Find the power spectrum for each array, and find the total power in the eight concentric box rings for each spectrum. Designate y_{ij} as the total power in the jth spectrum box ring of the ith of the four arrays in the right-most 60 percent of the data area, and designate x_{ij} as the same quantity for the remaining four arrays ($i = 1, 2, 3, 4$ and $j = 1, 2, \ldots, 8$).

(c) Solve the matrix equation $w'Mc = d$ for c, where M is the 8 by 8 matrix that has x_{ij} as its first four rows and y_{ij} as its last four rows, $c = (c_1, c_2, \ldots, c_8)'$ is a vector of unknown coefficients, $d = (1, 1, 1, 1, 0, 0, 0, 0)'$ is a vector of dummy variables, and $w = (1/4, 1/12, \ldots, 1/62)'$ is a vector of weights that equalizes the areas of the spectrum box rings.

(d) Form a set of eight ring boxes with each box assigned a successive coefficient value; the result is the synthesized adaptive filter.

Figure 11 shows the synthesized adaptive filter and its impulse response. Figure 12 locates the eight training regions (boxes) on the optical data before processing and shows the optical data after processing with the adaptive filter. Figure 13 shows this data as a contour plot and also displays the inner product zc as a gray-scale plot, where z is an eight-element vector of box ring powers for all possible 16 by 16 pixel arrays in two pixel increments. It is clear from Figures 12 and 13 that the adaptive filter is not effective in distinguishing the relatively uncorroded right-most 60 percent of the data area from the remaining area.

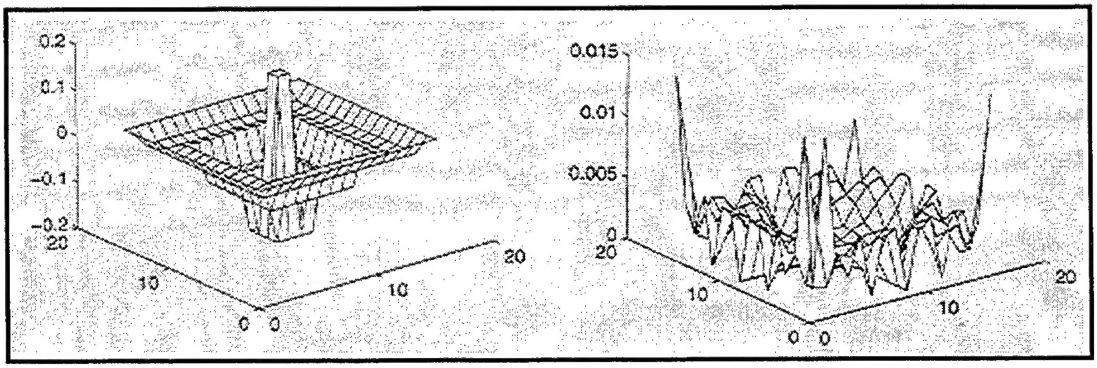

Figure 11. Synthesized Adaptive Filter (left), Corresponding Impulse Response (right).

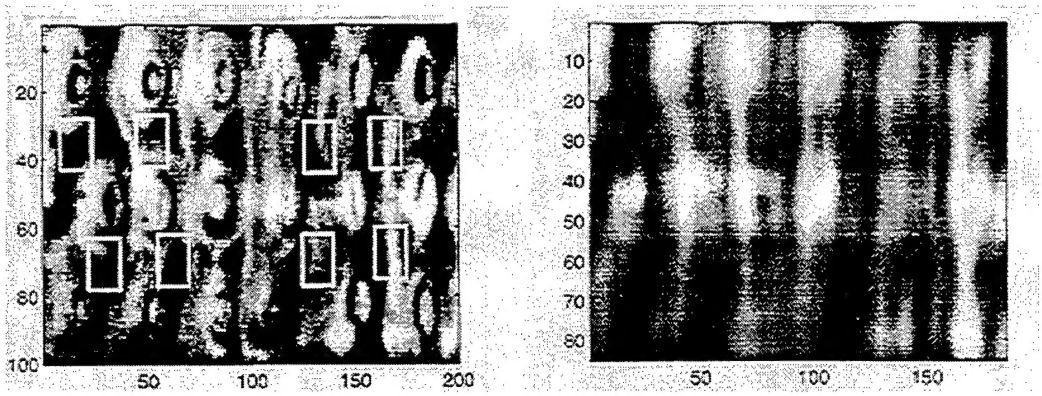

Figure 12. Eight Training Regions (Boxes) on Optical Data Before Processing (left), Optical Data After Processing with Adaptive Filter (right).

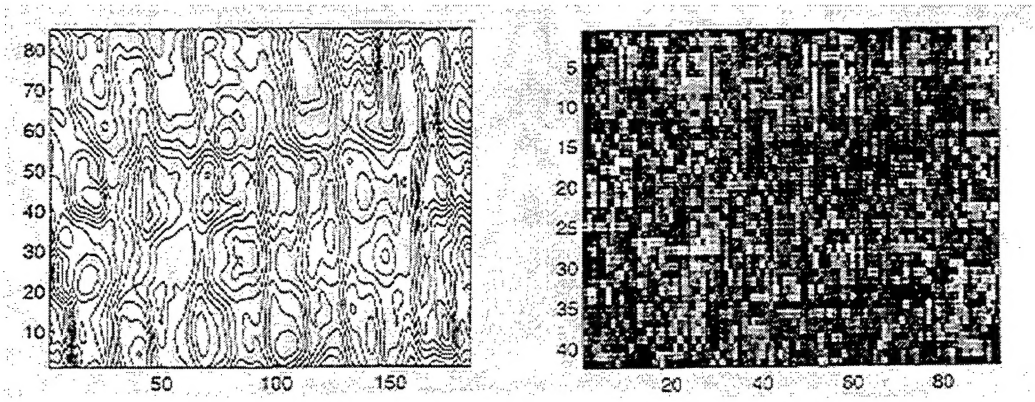

Figure 13. Contour Plot (12 Contours) of Optical Data After Processing with Adaptive Filter (left), Gray Scale Plot of Inner Product ZC (right).

CONCLUSION

Neither standard static spatial frequency filters nor adaptive filters synthesized using neural network technology appear to be effective for identifying corrosion damage in an aircraft lap joint coupon using available optical data. As indicated in Section 2 above, qualitative visual assessment of the optical data reveals no apparent distinction between corroded and uncorroded areas. The human visual system can function as an exceptionally powerful neural network pattern recognizer, and thus the inability of this system to identify any distinctive pattern in the optical data that correlates with actual corrosion (as determined by the x-ray data) may be ominous for the success of any artificial neural network technology applied to the same data. Perhaps data from other test coupons for which possibly different corrosion processes could produce more pronounced "pillowing," would yield more positive results.

REFERENCES

Howard, M., Mitchell, G., and Tietz, H. (1995). *Development of Procedures for Using Nondestructive Inspection Equipment to Detect Hidden Corrosion on USAF Aircraft.* ARINC Inc. report for OC-ALC/TIES under USAF contract F41608-93-D-0649.

Karpala F. and Hageniers, O. (1995). *Development of a D-SIGAT Aircraft Inspection System: Phase II.* (Report TP12470E), Diffracto Ltd., 2835 Kew Dr., Windsor, ON, Canada.

O'Keefe, C., Mayton, D. , Alcott, J., Dougan, K., and Howard, M. (1995). *Results of Evaluation of Nondestructive Inspection Equipment for Long-Term Use to Detect Hidden Corrosion on Aging Aircraft Systems.* ARINC Inc. report for OC-ALC/TIES under USAF contract F41608-90-D-0544-SD01-04.

Ripley, B. D. (1996). *Pattern Recognition and Neural Networks.* Cambridge Univ. Press.

LIST OF ABBREVIATIONS, ACRONYMS, AND SYMBOLS

AL	Armstrong Laboratory
WL	Wright Laboratory
ARINC	Aeronautical Radio, Inc.